Heliyon

ELSEVIER

Received:
16 May 2016
Revised:
9 September 2016
Accepted:
21 September 2016

Heliyon 2 (2016) e00171

Synthesis of magnetic alloy-filling carbon nanoparticles in super-critical benzene irradiated with an ultraviolet laser

Yasuhiro Hayasaki [a], **Takashi Hasumura** [b], **Takahiro Fukuda** [b], **Yutaka Nagaoka** [b], **Tomofumi Ukai** [b], **Seiki Iwai** [a], **Takashi Uchida** [a,b], **Toru Maekawa** [a,b,*]

[a] *Graduate School of Interdisciplinary New Science, Toyo University, 2100, Kujirai, Kawagoe, Saitama 350-8585, Japan*

[b] *Bio-Nano Electronics Research Centre, Toyo University, 2100, Kujirai, Kawagoe, Saitama 350-8585, Japan*

* Corresponding author.

E-mail address: maekawa@toyo.jp (T. Maekawa).

Abstract

Magnetic nanoparticles are of great importance particularly in the field of biomedicine as well as nanotechnology and nano materials science and technology. Here, we synthesise magnetic alloy-filling carbon nanoparticles (MA@C NPs) via the following two-step procedure; (1) Irradiation of a laser beam of 266 nm wavelength into super-critical benzene, in which both ferrocene and cobaltocene are dissolved, at 290 °C; and (2) annealing of the particles at 600 and 800 °C. We find that the core particles are composed of cobalt (Co), iron (Fe) and oxygen (O) and covered with carbon layers. The structure of the core particles as-synthesised, and annealed at 600 and 800 °C, is, respectively, amorphous, $CoFe_2O_4$ and FeCo. We also investigate the viability of L929 cells in the presence of MA@C NPs and find that there is no serious advert effect of the MA@C NPs on the cell viability thanks to the carbon layers covering the core particles. The magnetic properties are well characterised. The saturation and remnant magnetisation and coercivity increase and as a result, the hyperthermic efficiency becomes higher with an increase in the annealing temperature. The further modification of the surface of

http://dx.doi.org/10.1016/j.heliyon.2016.e00171

the present particles with several functional molecules becomes easier due to the carbon layers, which makes the present particles more valuable. It is therefore supposed that the presently synthesised MA@C NPs may well be utilised for nanotechnology-based biomedical engineering; e.g., nano bioimaging, nano hyperthermia and nano surgery.

Keywords: Engineering, Physical chemistry, Inorganic chemistry, Materials science

1. Introduction

Magnetic nanoparticles have attracted a lot of attention in recent years considering particularly their application to biomedical studies; e.g., they can be used as nano agents for the enhancement of magnetic resonance imaging, nano media for hyperthermic treatment of cancer cells, nano vehicles for drug delivery and nano robots for the encouragement of biochemical reactions and surgery on target cells [1, 2, 3, 4, 5, 6, 7, 8, 9]. Heat is generated in magnetic nanoparticles by applying alternating magnetic fields to them via either the Néel or hysteresis loss heating effect depending on the magnetic nature of nanoparticles; i.e., superparamagnetism or ferromagnetism [10]. Hyperthermic treatment of cancer cells using magnetic nanoparticles subjected to alternating magnetic fields has been actively studied in recent years since only target cells can be locally heated and killed without damaging any other normal cells [11, 12, 13, 14]. Biocompatibility of nanoparticles, however, becomes a crucial factor when they are used for medical treatment, noting that metallic particles are in general cytotoxic [15, 16]. The size of particles is also important when the particles are used for biomedical purposes [17, 18]. It should also be noticed that the efficiency of hyperthermic treatment of cells depends on the magnetic nature of the particles and the magnetic properties; that is, the saturation and remnant magnetisation, and coercivity [19].

Magnetic materials such as iron, cobalt and nickel are appropriate candidates for hyperthermic treatment of cells, but the biocompatibility, size and magnetic properties of the particles become crucial factors as mentioned. Carbon materials are generally speaking chemically stable and biocompatible compared to metal particles [20] and therefore it is demanded to produce biocompatible magnetic nanoparticles covered with carbon layers.

The gas-liquid coexistence curves terminate at the critical points, where large molecular clusters are formed and several critical anomalies such as divergence of the physical properties and fast propagations of temperature, pressure and density perturbations; known as the piston effect, occur [21]. It has also been demonstrated that nano materials can be efficiently synthesised in near-critical and super-critical fluids such as carbon dioxide, benzene and acetone under their near- and super-

http://dx.doi.org/10.1016/j.heliyon.2016.e00171

critical conditions, by irradiating ultraviolet (UV) laser beams into the fluids [22, 23, 24, 25].

Here, we synthesise magnetic alloy-filling carbon nanoparticles (MA@C NPs) via the following two-step procedure; i.e., (1) irradiation of a UV laser beam into super-critical benzene, in which both ferrocene ($Fe(cp)_2$) and cobaltocene ($Co(cp)_2$) are dissolved, at 290 °C; and (2) annealing of the particles at 600 and 800 °C. The magnetic properties, cytotoxicity and hyperthermic ability of the MA@C NPs are also examined. The experimental details are summarised in the second section. The results of the experiments are discussed in the third section and the results obtained in the present study are summarised in the final section.

2. Materials and methods

2.1. Synthesis of MA@C NPs

An outline of the experimental system is shown in Fig. 1. Benzene, in which both $Fe(cp)_2$ and $Co(cp)_2$ were dissolved, was confined in a cylindrical container made of stainless steel. The inner and outer diameters, and inner and outer heights of the container were, respectively, 13 and 60 mm, and 23 and 66 mm. The density of benzene was set at its critical value and the concentration of $Fe(cp)_2$ and $Co(cp)_2$ in benzene was set at 200 and 15 mg mL^{-1}; i.e., 1.08 and 0.08 mM mL^{-1}, respectively. A synthetic quartz window was mounted at the bottom of the container for the introduction of a laser beam. The diameter and thickness of the synthetic quartz window was 20 and 10 mm. A platinum resistance thermometer (Pt100, Chino Co. Ltd.) was set in the container wall and the temperature of the fluid was regulated by a heater, which was installed around the container, and a

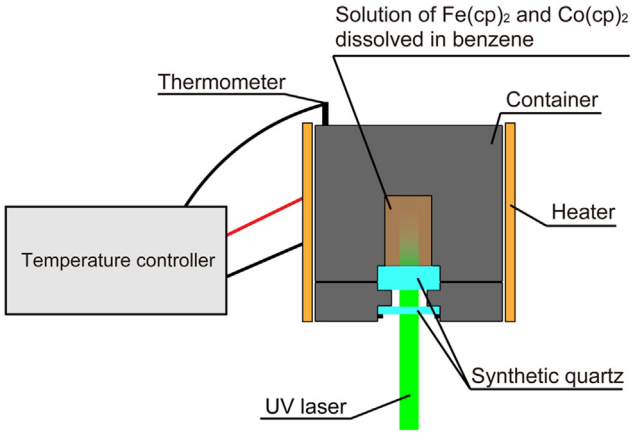

Fig. 1. Outline of the experimental system. Benzene, in which metallocenes such as ferrocene and cobaltocene are dissolved, is confined in a cylindrical container made of stainless steel. The density and temperature of benzene are, respectively, set at its critical value and 290 °C. A laser beam of 266 nm wavelength is irradiated into the solution.

http://dx.doi.org/10.1016/j.heliyon.2016.e00171

temperature controller (LT470, Chino Co. Ltd.). The fluid conditions were changed from a gas-liquid two-phase region at 25 °C to super-critical one at 290 °C by controlling the fluid temperature. Note that the critical temperature T_c, pressure P_c and density ρ_c of benzene are 289 °C, 4.92 MPa and 302 kg m^{-3} [26]. 50000 pulses of a UV laser beam of 266 nm wavelength were irradiated from a neodymium doped yttrium/aluminium/garnet (Nd:YAG) laser (Brilliant Quantel Ltd. Co.) into the solution of $Fe(cp)_2$ and $Co(cp)_2$ dissolved in benzene. The diameter and energy flux of the laser beam were, respectively, 10 mm and 3.8 mW mm^{-2}. The duration of each laser pulse and the frequency of the pulse generation were 4.3 ns and 10Hz. The beam was not focused on any particular point. After UV laser irradiation, the temperature of the fluid was decreased gradually down to room temperature switching the heater off and then the fluid was released. The particles produced in the container were separated using a neodymium magnet, washed five times with ethanol and dried in a vacuum evaporator for 24 h. The particles were annealed in a thermogravimetric analyser (TGA) (DTG-60H, Shimadzu) under a constant flow of argon, increasing the temperature from 25 up to either 600 or 800 °C at a rate of 20 °C min^{-1}. Once the temperature reached the target value; that is, 600 or 800 °C, the temperature was kept at 600 or 800 °C for 1 min and the particles were cooled naturally down to room temperature in the TGA.

2.2. Structural, elemental and magnetic characterisation of NPs

The structures of the particles were observed and analysed by transmission electron microscopy (TEM) (JEM-2200FS, JEOL), X-ray diffractometry (XRD) (SmartLab (9 kW)-RPA, Rigaku Corp.) and Raman spectroscopy (LabRAM, HR-800, HORIBA JOBIN YVON S.A.S). The elemental components of the structures were analysed by energy-disperse X-ray spectroscopy (EDS) (JED-2300T, JEOL). The size of the particles was measured from TEM images, targeting at least 1000 particles synthesised under the same experimental conditions. The magnetic properties of the particles were measured by a superconducting quantum interference device (SQUID) magnetometer (MPMS3, Quantum Design, Inc.). The zero field cooling (ZFC) and field cooling (FC) magnetisation curves of particles as-synthesised, and annealed at 600 and 800 °C were obtained in the temperature range between 2.0 and 400 K in an applied field of 100 Oe (= $10^5/4\pi$ A m^{-1}). The mass magnetisation − magnetic field curves were also obtained at 4 and 300 K.

2.3. Cell viability evaluation of NPs by an Alamar blue assay

A test cell line; L929 (Cat EC85011425-FO, DS Pharma Biomedical Co., Ltd.), was cultivated in a 25 cm^3 flask, which contained Dulbecco's modified eagle media (DMEM) (Gibco, Life Technologies) supplemented with 10% foetal bovine serum and 1% penicillin-streptomycin. The cells were seeded in 96-well plates with

http://dx.doi.org/10.1016/j.heliyon.2016.e00171

DMEM at a cell number density of 2×10^3 cells per well (CPW) and incubated for 24 and 48 h. Then, the media were removed and replaced by fresh ones and the cells of 2×10^3 CPW were incubated in the presence of a different concentration of particles; 0, 10, 20, 40, 60, 80 and 100 μg mL^{-1}, followed by treatment with an Alamar blue reagent for 3 h. The incubation was performed in an atmosphere of 5% CO_2 at 37 °C. The fluorescence of the solution was then measured to evaluate the cell viability using a fluorescence imager (Typhoon FLA 7000, GE Healthcare Life Science Ltd.) with an excitation wavelength of 532 nm. The cells in the media in the absence of particles acted as the positive control. Statistical analysis was performed using the one-way ANOVA and the Turkey-Kramer multiple comparison *post hoc* test (Social Survey Research Information Co. Ltd.) and the significant level was set at 0.01. The results were presented as mean ± standard deviation.

2.4. Evaluation of hyperthermic performance

We carried out some preliminary experiment to investigate the hyperthermic performance of the nanoparticles dispersed in ethanol. The concentration of the nanoparticles in the solution was set at 0.5 mg mL^{-1}. The solution was introduced into a 1 mL test tube, which was placed at the centre of an induction heating coil (EASYHeat 8310 LI, Ambrell An American Co.). An ac magnetic field, the frequency and strength of which were 331 kHz and 47.9 kA m^{-1}, was applied for 5 min. The surface temperature of the solution was measured by a radiation thermometer (Testo855, Testo Co. Ltd.), which was set 100 mm above the surface of the solution in the test tube.

3. Results and discussion

We synthesised NPs by irradiating a laser beam of 266 nm wavelength into benzene, in which both $Fe(cp)_2$ and $Co(cp)_2$ were dissolved, under its super-critical conditions at 290 °C, and then annealing the particles at 600 and 800 °C, as mentioned. Fig. 2, Fig. 3 and Fig. 4 show TEM images, EDS mappings and XRD diffractometry of particles produced via the interactions between the laser beam, and the solutes and benzene molecules. The TEM images clearly show that the core particles as-synthesised (see Fig. 2(a) and Fig. 3(A)), and annealed at 600 (Fig. 2(b) and Fig. 3(B)) and 800 °C (Fig. 2(c) and Fig. 3(C)) are covered with some layers in all of the cases. According to the TEM, EDS, and XRD analyses on the elements and structures of the particles, the core particles were composed of Co, Fe and O and covered with a mixture of graphitic and amorphous carbon layers (see Fig. 2, Fig. 3 and Fig. 4). As shown in Fig. 4, there is a low peak at a diffraction angle of 44.85° in the case of NPs as-synthesised (Fig. 4(a)) and therefore the structure of the core particles is mostly amorphous. In the case of NPs annealed at 600 °C (Fig. 4(b)), three peaks at a diffraction angle of 45.01°, 65.57°

http://dx.doi.org/10.1016/j.heliyon.2016.e00171

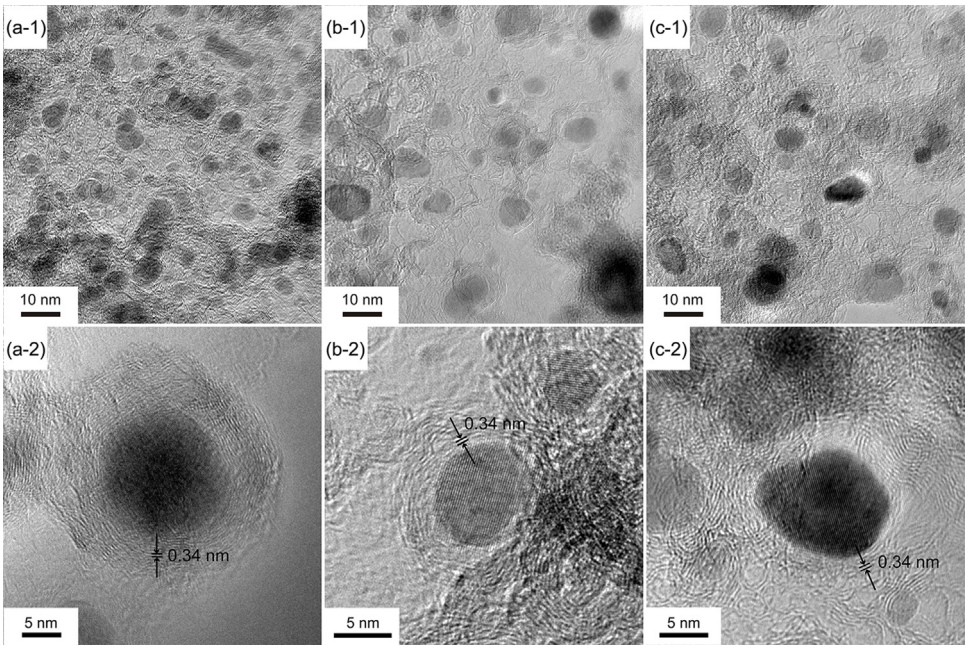

Fig. 2. TEM images of NPs. (a) NPs as-synthesised. (b) NPs annealed at 600 °C. (c) NPs annealed at 800 °C. The core particles are covered with carbon layers.

and 82.97 ° corresponding, respectively, to the crystal planes of (110), (200) and (211) of FeCo alloys. The D-spacing is 0.201, 0.142 and 0.116 nm. The other peaks at a diffraction angle of 30.19°, 35.60°, 57.06° and 62.74 ° correspond to the crystal planes of (220), (311), (511) and (440) of $CoFe_2O_4$. The D-spacing is 0.295, 0.208, 0.161 and 0.147 nm. In the case of NPs annealed at 800 °C (Fig. 4(c)), three peaks at a diffraction angle of 44.75°, 65.22° and 82.52 ° correspond to the crystal planes of (110), (200) and (211) of FeCo. The D-spacing is 0.202, 0.142 and 0.116 nm. The other peaks at a diffraction angle of 30.17°, 35.52°, 57.2° and 62.9 ° correspond to the crystal planes of (220), (311), (511) and (440) of $CoFe_2O_4$. The D-spacing is 0.298, 0.253, 0.16 and 0.147 nm. In summary, most of the core structures of as-synthesised particles were amorphous, whereas clear peaks corresponding to FeCo, $CoFe_2O_4$ and Co appearing in the particles annealed at 600 and 800 °C, it is supposed that the degree of the crystallinity of the core particles increased with an increase in the annealing temperature. Note that $CoFe_2O_4$ particles were produced due to oxygen molecules dissolved in benzene, whereas Co particles were synthesised via both pyrolytic [27] and photolytic decomposition of $Co(cp)_2$. The weight percentages of FeCo, $CoFe_2O_4$ and Co were 9.5, 85.0 and 5.1% when the particles were annealed at 600 °C, whereas those were 83.9, 10.5 and 5.5% when the particles were annealed at 800 °C, according to the reference intensity ratio values (ICDD 01-077-7452, 01-071-7171 and 01-074-6402). In other words, the composition of the core particles can be changed depending on the annealing temperature; that is, the core particles are mainly composed of $CoFe_2O_4$

http://dx.doi.org/10.1016/j.heliyon.2016.e00171

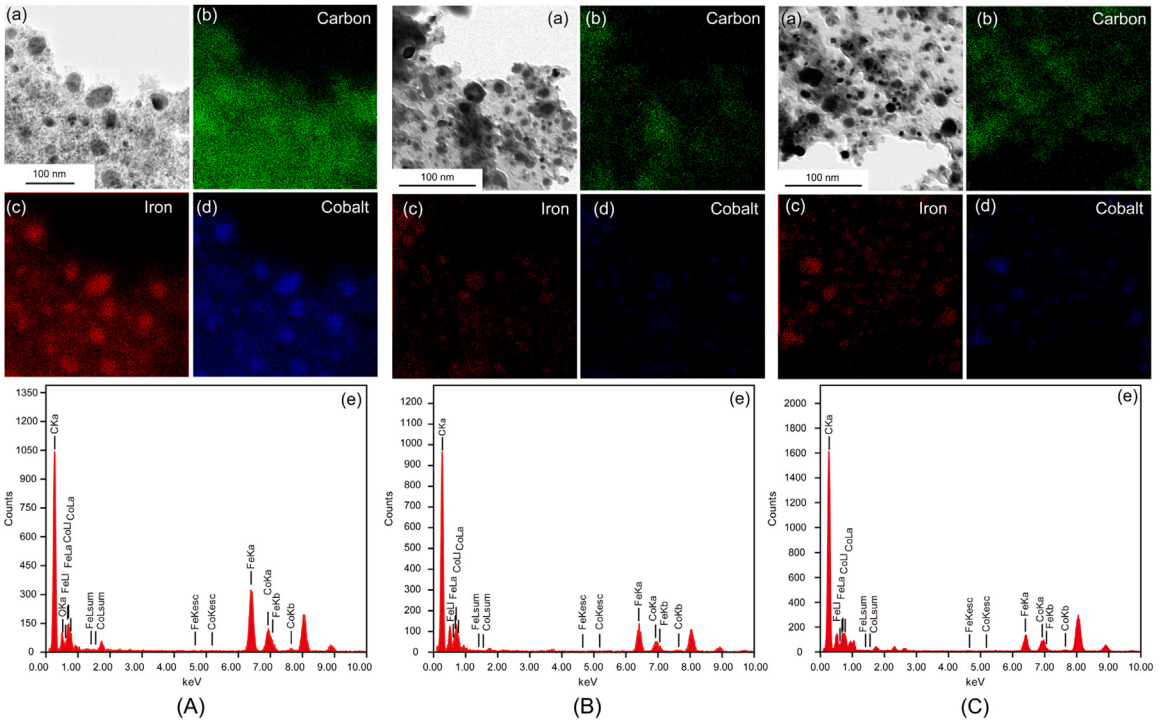

Fig. 3. TEM images and EDS mappings of NPs. (A) NPs as-synthesised. (a) TEM image; (b) EDS mapping of carbon corresponding to (a); (c) EDS mapping of iron corresponding to (a); (d) EDS mapping of cobalt corresponding to (a); (e) EDS energy peaks. (B) NPs annealed at 600 °C. (a) TEM image; (b) EDS mapping of carbon corresponding to (a); (c) EDS mapping of iron corresponding to (a); (d) EDS mapping of cobalt corresponding to (a); (e) EDS energy peaks. (C) NPs annealed at 800 °C. (a) TEM image; (b) EDS mapping of carbon corresponding to (a); (c) EDS mapping of iron corresponding to (a); (d) EDS mapping of cobalt corresponding to (a); (e) EDS energy peaks.

at 600 °C, while they are composed of FeCo at 800 °C [28]. The layers covering the core particles were composed of a mixture of graphitic carbon layers, where the gap between two adjacent sheets was 0.34 nm [29], and amorphous carbon (see Fig. 2). Raman spectra of the NPs as-synthesised and annealed at 600 and 800 °C

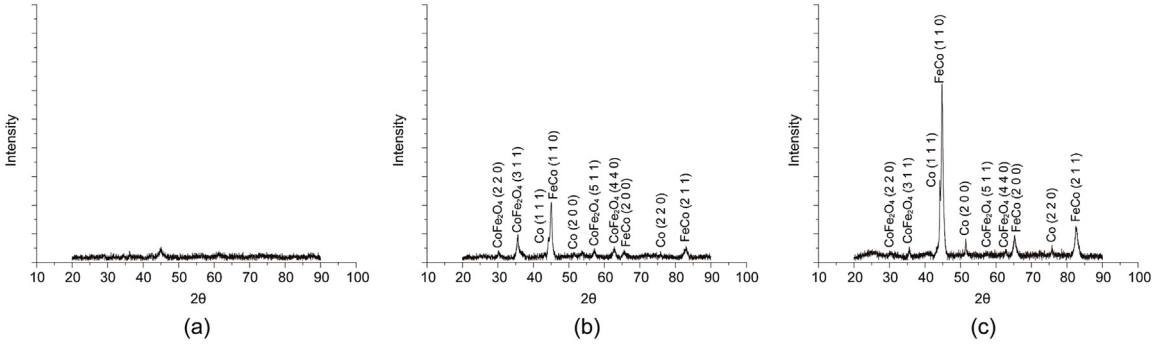

Fig. 4. X-ray diffractogram of NPs. (a) NPs as-synthesised. (b) NPs annealed at 600 °C. (c) NPs annealed at 800 °C.

http://dx.doi.org/10.1016/j.heliyon.2016.e00171

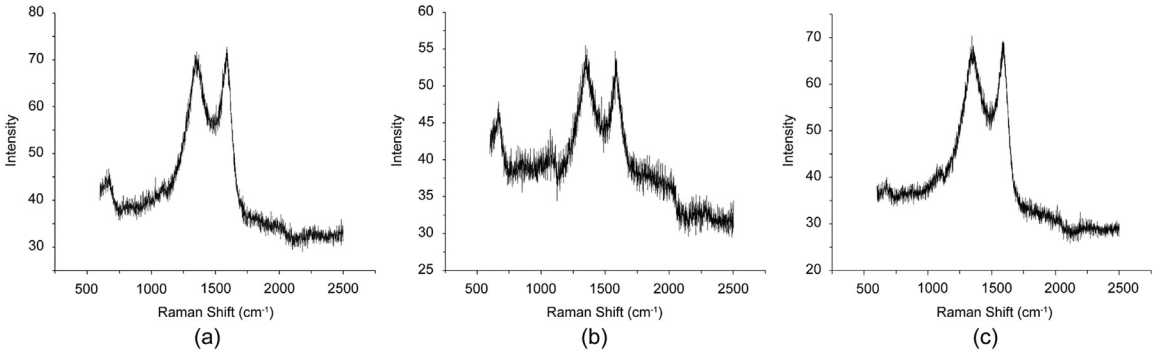

Fig. 5. Raman spectra. (a) NPs as-synthesised. (b) NPs annealed at 600 °C. (c) NPs annealed at 800 °C.

are shown in Fig. 5. In all of the cases, peaks corresponding to the G and D bands appeared and there was no appreciable change in the spectra before and after annealing. In other words, there was no distinct effect of annealing on the structure of the carbon layers covering the core particles since the temperature was kept at 600 or 800 °C for only 1 min after it had been increased at a rate of 20 °C min^{-1}.

We measured the equivalent diameter of the core particles; $(l + s)/2$, based on the long and short axes; l and s, and the thickness of the carbon layers covering the core particles from TEM images, targeting at least 1000 particles produced under the same experimental conditions. The diameter of the core particles as-synthesised and annealed at 600 and 800 °C was, respectively, 4.8 ± 2.1, 5.5 ± 2.4 and 6.5 ± 2.5 nm, whereas the thickness of the carbon layers was 1.9 ± 0.6, 2.0 ± 0.6 and 2.5 ± 0.7 nm (see Fig. 6 for the distribution of the size of the core particles and the thickness of the carbon layers). The diameter of the core particles and the thickness of the carbon layers increased with an increase in the annealing temperature. It is supposed that the diameter of the core particles increased during the annealing process of the particles via the Ostwald ripening effect; that is, iron and cobalt atoms in smaller core particles diffused outwards through the carbon layers and were eventually absorbed by neighbouring larger particles [30, 31]. We suppose that the thickness of the carbon layers increased with an increase in the annealing temperature since carbon atoms dissolved in the core particles diffused outwards into the carbon layers [32].

Iron and cobalt composing the core particles were, respectively, dissociated from $Fe(cp)_2$ and $Co(cp)_2$, whereas carbon covering the core particles was dissociated from $Fe(cp)_2$, $Co(cp)_2$ and benzene molecules. As explained previously, benzene molecules, $Fe(cp)_2$ and $Co(cp)_2$ are quite easily dissociated via the interactions between photons of 266 nm wavelength, and benzene, $Fe(cp)_2$ and $Co(cp)_2$ molecules [33, 34, 35, 36, 37]. At least two-photon absorption is required for the dissociation of a hydrogen atom from a benzene molecule, knowing that the dissociation energy and the photon energy of 266 nm wavelengths are,

http://dx.doi.org/10.1016/j.heliyon.2016.e00171

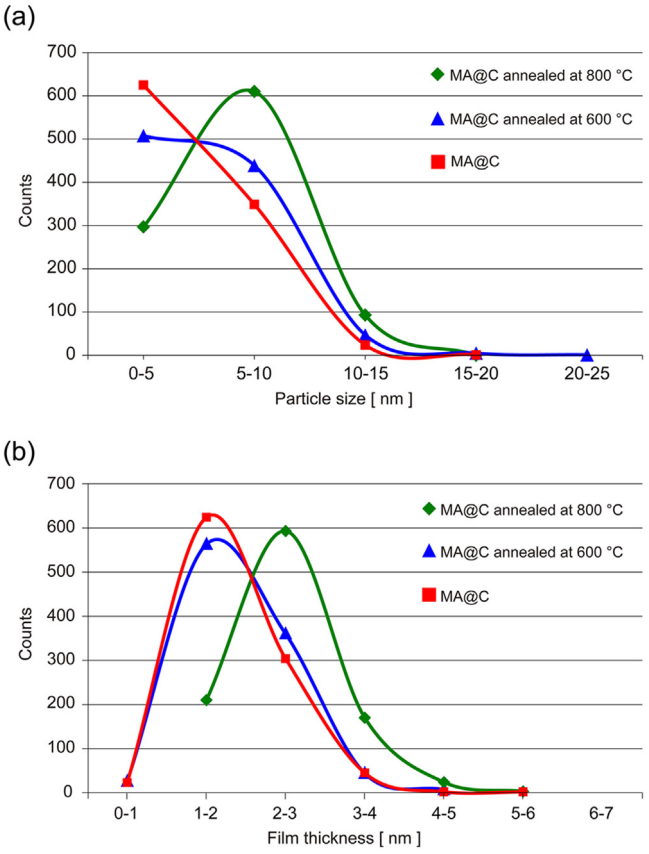

Fig. 6. Distribution of the diameter of a core particle and the thickness of a layer covering the core particle. (a) Diameter of NPs as-synthesised, annealed at 600 °C and annealed at 800 °C. (b) Thickness of a layer covering the core particle as-synthesised, annealed at 600 °C and annealed at 800 °C.

respectively, 4.90 and 4.66 eV [38]. It is also known that the dissociation energy of a second hydrogen atom is lower than that of the first one [38] and therefore six-membered rings of carbon atoms may be quite easily produced by irradiation of photons of 266 nm wavelength, noting that the possibility of multi-photon absorption increases as the state of benzene approaches its critical point due to the formation of large flexible molecular clusters [38]. The decomposition energy of $Fe(cp)_2$ into Fe + cp + cp is 6.8 eV [39], whereas that of $Co(cp)_2$ into Co + cp + cp is 5.64 eV [40] and therefore the decomposition of ferrocene and cobaltocene into iron, cobalt and cp-rings was induced by two-photon absorption during the laser irradiation. Dissociated iron and cobalt atoms were cooled to form the core particles and the carbon layers covering the core particles were formed by cp-rings and six-membered rings of carbon atoms during the interval between two pulses of laser beams [41].

The ZFC/FC magnetisation curves measured changing the temperature between 2.0 and 400 K are shown in Fig. 7, where an external magnetic field of 100 Oe ($= 10^5/4\pi$ A m^{-1}) was applied after the ZFC measurement. It is clearly shown that

http://dx.doi.org/10.1016/j.heliyon.2016.e00171

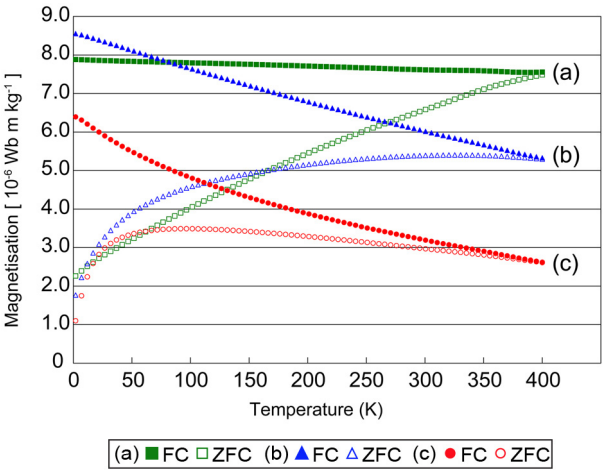

Fig. 7. FC-ZFC curves of NPs measured between 2 and 400 K. (a) NPs annealed at 800 °C. (b) NPs annealed at 600 °C. (c) NPs as-synthesised.

there was no transition from ferromagnetism to superparamagnetism down to 2 K and from ferromagnetism to paramagnetism up to 400 K. The mass magnetisation – magnetic field curves measured at 300 and 4 K are shown in Fig. 8. The saturation and remnant magnetisation and coercivity of particles as-synthesised, and annealed at 600 and 800 °C are summarised in Table 1. The saturation and remnant magnetisation and coercivity increased with an increase in the annealing temperature. Particles annealed at 600 and 800 °C showed ferromagnetic characteristics caused by strong dipole-dipole interactions among particles, whereas particles as-synthesised was soft ferromagnetic. The saturation and remnant magnetisation and coercivity of MA@C NPs annealed at 800 °C were higher than those of iron-filling and cobalt-filling carbon nanoparticles (Fe@C NPs and Co@C NPs) [29], noting that the magnetic performance of alloys are often superior to that of materials composed of a single element.

We examined the viability of cell line L929 in the presence of MA@C NPs as-synthesised, and annealed at 600 and 800 °C using an Alamer blue assay, where the concentration of MA@C NPs was set at 10, 20, 40, 60, 80 and 100 μg mL^{-1} and the incubation time was 24 and 48 h. The result of the Alamer blue assay is shown in Fig. 9. The cell viability was over 80% when the incubation time was 24 h, whereas it was between 70 and 80% in the case of 48 h incubation. It is supposed that the cell viability was not seriously deteriorated due to the carbon layers covering the core particles [42]. Note that there was no significant effect of the annealing temperature on the structures of the carbon layers covering the core particles (see Fig. 5) and therefore the cell viability in the presence of MA@C NPs as-synthesised, and annealed at 600 and 800 °C was more or less the same.

http://dx.doi.org/10.1016/j.heliyon.2016.e00171

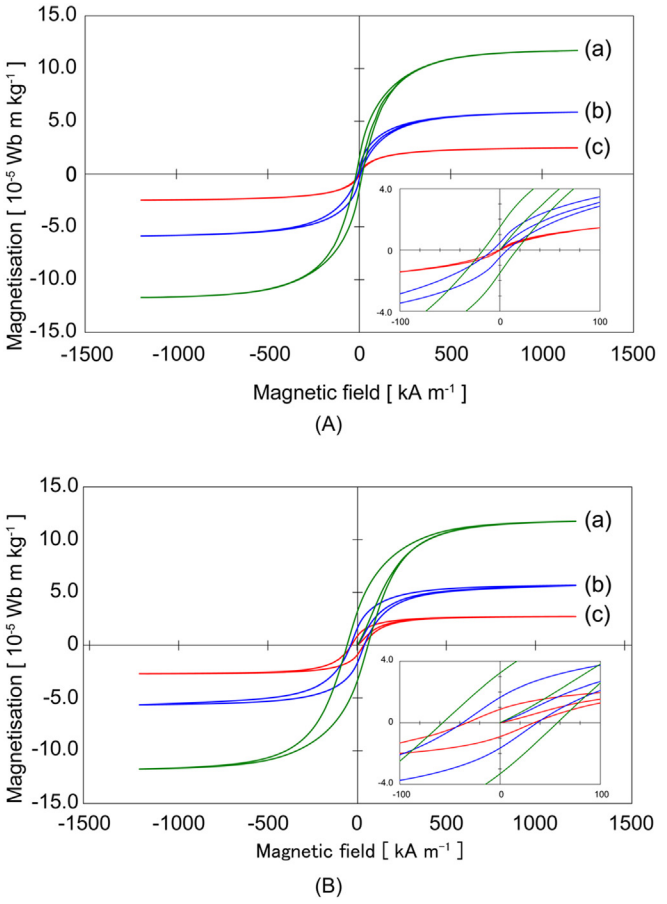

Fig. 8. Mass magnetisation-magnetic field curves measured at 300 and 4 K. (A) Mass magnetisation-magnetic field curves measured at 300 K. (a) NPs annealed at 800 °C; (b) NPs annealed at 600 °C; (c) NPs as-synthesised. (B) Mass magnetisation-magnetic field curves measured at 4 K. (a) NPs annealed at 800 °C; (b) NPs annealed at 600 °C; (c) NPs as-synthesised.

Table 1. Magnetic properties of MA@C NPs.

	Measurement temperature	**Saturation magnetisation [Wb m kg^{-1}]**	**Remnant magnetisation [Wb m kg^{-1}]**	**Coercivity [A m^{-1}]**
NPs as-synthesised	300 K	2.5×10^{-5}	2.5×10^{-7}	0.8
	4 K	2.7×10^{-5}	8.9×10^{-6}	3.4×10
NPs annealed at 600 °C	300 K	5.9×10^{-5}	4.8×10^{-6}	7.6
	4 K	5.7×10^{-5}	1.7×10^{-5}	3.8×10
NPs annealed at 800 °C	300 K	1.2×10^{-4}	1.5×10^{-5}	1.7×10
	4 K	1.2×10^{-4}	3.2×10^{-5}	5.7×10

http://dx.doi.org/10.1016/j.heliyon.2016.e00171

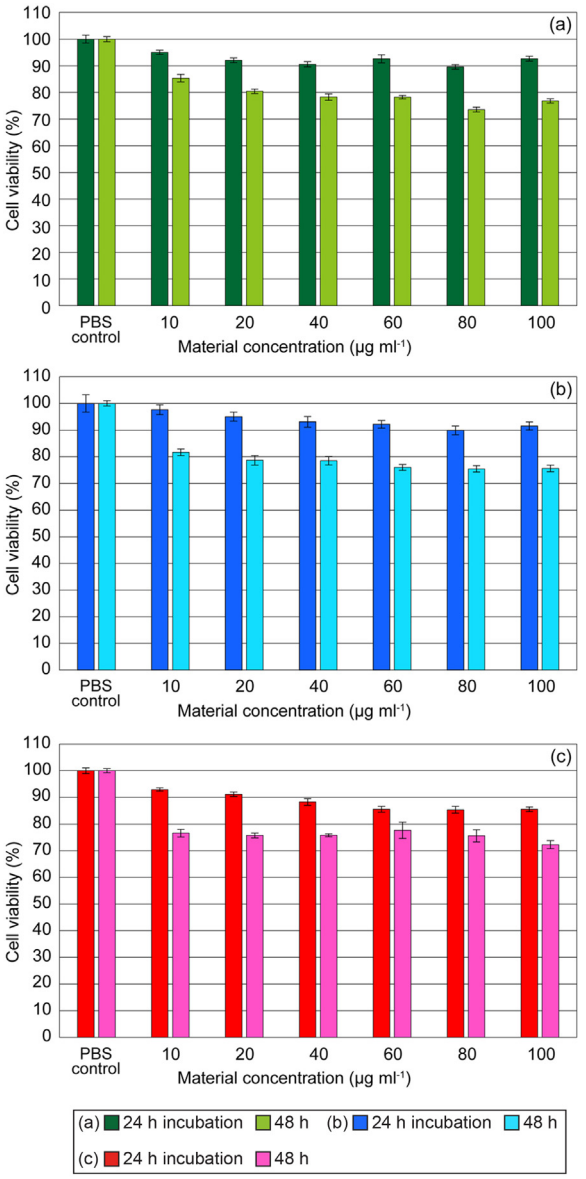

Fig. 9. Viability of cell line L929. (a) Cell viability in the presence of NPs annealed at 800 °C. (b) Cell viability in the presence of NPs annealed at 600 °C. (c) Cell viability in the presence of NPs as-synthesised.

The time variation of the surface temperature of the solution of MA@C NPs dispersed in ethanol (0.5 mg mL^{-1}) is shown in Fig. 10. The temperature of the solution increased rapidly when the MA@C NPs annealed at 800 °C were used. The strength of the external ac magnetic field was changed between $\pm$ 47.9 kA m^{-1} as mentioned and therefore we measured the mass magnetisation – magnetic field curves of MA@C NPs, changing the magnetic field between $\pm$ 47.9 kA m^{-1}, the result of which is shown in Fig. 11. Hysteresis loops were also obtained in all of the cases. The heating mechanism of the particles has not yet been clearly

http://dx.doi.org/10.1016/j.heliyon.2016.e00171

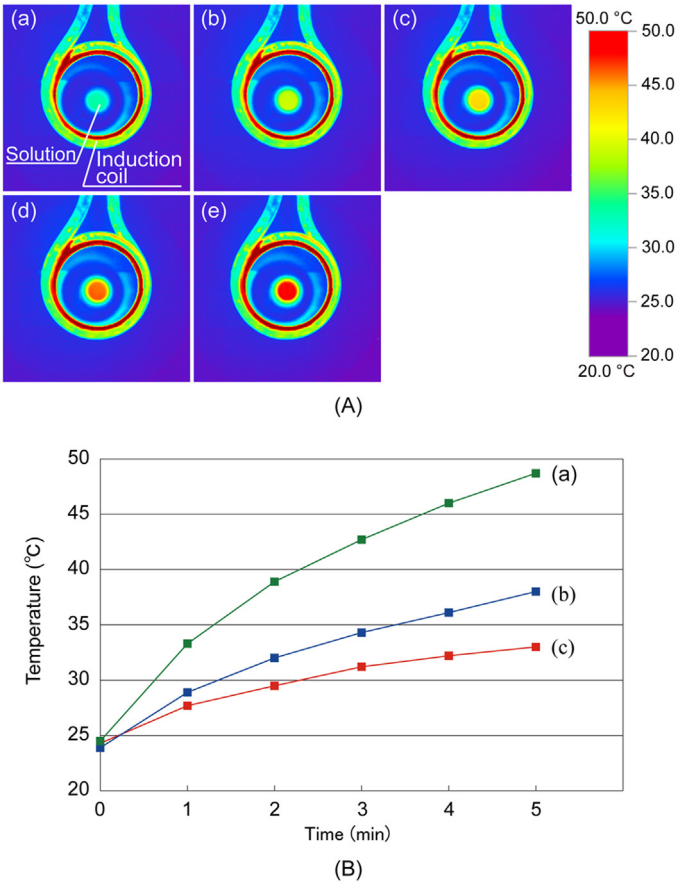

Fig. 10. Time variation of the surface temperature of the solution of NPs dispersed in ethanol. (A) Time variation of the surface temperature of the solution of NPs annealed at 800 °C. (a) 1 min after the initiation of induction heating; (b) 2 min; (c) 3 min; (d) 4 min; (e) 5 min. (B) Time variation of the surface temperature of the solution of NPs. (a) NPs annealed at 800 °C; (b) NPs annealed at 600 °C; (c) NPs as-synthesised.

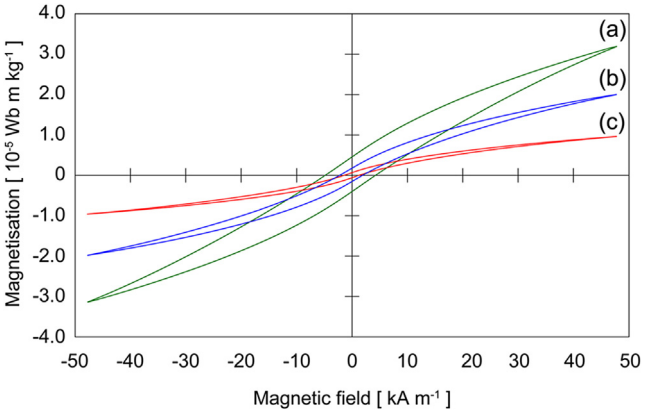

Fig. 11. Magnetisation-magnetic field curves of NPs measured at 300 K. The strength of the external magnetic field was changed between ± 47.9 kA m^{-1} following the hyperthermic experimental conditions. (a) NPs annealed at 800 °C; (b) NPs annealed at 600 °C; (c) NPs as-synthesised.

http://dx.doi.org/10.1016/j.heliyon.2016.e00171

understood, but we suppose that the particles were heated via the Néel effect in each particle and hysteresis loss heating caused by the dipole-dipole interactions among the particles.

4. Conclusions

We synthesised magnetic alloy-filling carbon nanoparticles via a two-step procedure; (1) A laser beam of 266 nm wavelength was irradiated into super-critical benzene, in which both ferrocene and cobaltocene are dissolved, at 290 °C; and (2) the particles were annealed at 600 and 800 °C. We found that the structure of the core particles as-synthesised was amorphous, whereas the composition of the core particles annealed at 600 and 800 °C, were, respectively, $CoFe_2O_4$ and FeCo. We also confirmed that there was no serious advert effect of the present nanoparticles on the cell viability due to the carbon layers covering the core particles. The saturation and remnant magnetisation and coercivity increased with an increase in the annealing temperature and as a result, those annealed particles showed high hyperthermic performance. The further modification of the surface of the present particles with several functional molecules becomes easier thanks to the carbon layers and therefore it is supposed that the presently synthesised nanoparticles may well be utilised for nanotechnology-based biomedical engineering; e.g., nano bioimaging, nano hyperthermia and nano surgery.

Declarations

Author contribution statement

Yasuhiro Hayasaki: Conceived and designed the experiments; Performed the experiments; Analyzed and interpreted the data; Wrote the paper.

Takashi Hasumura: Conceived and designed the experiments; Performed the experiments; Analyzed and interpreted the data.

Takahiro Fukuda: Conceived and designed the experiments; Analyzed and interpreted the data.

Yutaka Nagaoka, Seiki Iwai: Performed the experiments; Analyzed and interpreted the data.

Tomofumi Ukai, Takashi Uchida: Analyzed and interpreted the data.

Toru Maekawa: Conceived and designed the experiments; Analyzed and interpreted the data; Contributed reagents, materials, analysis tools or data; Wrote the paper.

http://dx.doi.org/10.1016/j.heliyon.2016.e00171

Funding statement

This work was supported by a Grant for the Programme for the Strategic Research Foundation at Private Universities (S1101017), Organised by the Ministry of Education, Culture, Sports, Science and Technology (MEXT), Japan.

Competing interest statement

The authors declare no conflict of interest.

Additional information

No additional information is available for this paper.

Acknowledgements

We would like to thank Mr Keiichi Hirakawa and Mr Haruyoshi Sato; Technical Managers of the Bio-Nano Electronics Research Centre, Toyo University, for their support of TEM observation of nanostructures.

References

[1] J. Gao, H. Gu, B. Xu, Multifunctional magnetic nanoparticles: design, synthesis, and biomedical applications, Acc. Chem. Res. 42 (2009) 1097–1107.

[2] Y.-w. Jun, J.-w. Seo, J. Cheon, Nanoscaling laws of magnetic nanoparticles and their applicabilities in biomedical sciences, Acc. Chem. Res. 41 (2008) 179–189.

[3] C. Sun, J.S. Lee, M. Zhang, Magnetic nanoparticles in MR imaging and drug delivery, Adv. Drug. Deliv. Rev. 60 (2008) 1252–1265.

[4] E. Mazario, N. Menéndez, P. Herrasti, M. Cañete, V. Connord, J. Carrey, Magnetic hyperthermia properties of electrosynthesized cobalt ferrite nanoparticles, J. Phys. Chem. C 117 (2013) 11405–11411.

[5] H. Morimoto, T. Ukai, Y. Nagaoka, N. Grobert, T. Maekawa, Tumbling motion of magnetic particles on a magnetic substrate induced by a rotational magnetic field, Phys. Rev. E 78 (2008) 021403.

[6] C. Gao, W. Li, H. Morimoto, Y. Nagaoka, T. Maekawa, Magnetic carbon nanotubes: Synthesis by electrostatic self-assembly approach and application in the bio-manipulations, J. Phys. Chem. B. 110 (2006) 7213–7220.

 http://dx.doi.org/10.1016/j.heliyon.2016.e00171

[7] B.G. Nair, Y. Nagaoka, H. Morimoto, Y. Yoshida, T. Maekawa, D.S. Kumar, Aptamer conjugated magnetic nanoparticles as nanosurgeons, Nanotechnology 21 (455102) (2010).

[8] T. Mizuki, M. Sawai, Y. Nagaoka, H. Morimoto, T. Maekawa, Activity of lipase and chitinase immobilized on superparamagnetic particles subjected to a rotational magnetic field, PLoS One 8 (2013) e66528.

[9] B.G. Nair, T. Fukuda, T. Mizuki, T. Hanajiri, T. Maekawa, Intracellular trafficking of superparamagnetic iron oxide nanoparticles conjugated with TAT peptide: 3-dimensional electron tomography analysis, Biochem. Biophys. Res. Commun. 421 (2012) 763–767.

[10] N. Frickel, M. Gottlieb, A.M. Schmidt, Hybrid nanocomposites based on superparamagnetic and ferromagnetic particles: A comparison of their magnetic and dielectric properties, Polymer 52 (2011) 1781–1787.

[11] M.M. Yallapu, S.F. Othman, E.T. Curtis, B.K. Gupta, M. Jaggi, S.C. Chauhan, Multi-functional magnetic nanoparticles for magnetic resonance imaging and cancer therapy, Biomaterials 32 (2011) 1890–1905.

[12] A. Jordan, R. Scholz, P. Wust, H. Fähling, R. Felix, Magnetic fluid hyperthermia (MFH): Cancer treatment with AC magnetic field induced excitation of biocompatible superparamagnetic nanoparticles, J. Magn. Magn. Mater. 201 (1999) 413–419.

[13] J. Overgaard, Effect of hyperthermia on malignant cells in vivo: A review and a hypothesis, Cancer 39 (1977) 2637–2646.

[14] M. Latorre, C. Rinaldi, Applications of magnetic nanoparticles in medicine: magnetic fluid hyperthermia, P. R. Health Sci. J. 28 (2009).

[15] K. Chatterjee, S. Sarkar, K. Jagajjanani Rao, S. Paria, Core/shell nanoparticles in biomedical applications, Adv. Colloid Interface Sci. 209 (2014) 8–39.

[16] M. Mahmoudi, A. Simchi, M. Imani, Cytotoxicity of uncoated and polyvinyl alcohol coated superparamagnetic iron oxide nanoparticles, J. Phys. Chem. C 113 (2009) 9573–9580.

[17] E. Frohlich, The role of surface charge in cellular uptake and cytotoxicity of medical nanoparticles, Int. J. Nanomed. 7 (2012) 5577–5591.

[18] O. Veiseh, C. Sun, C. Fang, N. Bhattarai, J. Gunn, F. Kievit, K. Du, B. Pullar, D. Lee, R.G. Ellenbogen, J. Olson, M. Zhang, Specific targeting of brain tumors with an optical/magnetic resonance imaging nanoprobe across the blood-brain barrier, Cancer Res. 69 (2009) 6200–6207.

 http://dx.doi.org/10.1016/j.heliyon.2016.e00171

[19] S.P. Sherlock, H. Dai, Multifunctional FeCo-graphitic carbon nanocrystals for combined imaging, drug delivery and tumor-specific photothermal therapy in mice, Nano Res. 4 (2011) 1248–1260.

[20] Z. Abdullaeva, E. Omurzak, C. Iwamoto, H.S. Ganapathy, S. Sulaimankulova, C. Liliang, T. Mashimo, Onion-like carbon-encapsulated Co, Ni, and Fe magnetic nanoparticles with low cytotoxicity synthesized by a pulsed plasma in a liquid, Carbon 50 (2012) 1776–1785.

[21] T. Maekawa, K. Ishii, Y. Shiroishi, H. Azuma, Onset of buoyancy convection in a horizontal layer of a supercritical fluid heated from below, J. Phys. A: Math Gen. 37 (2004) 7955.

[22] T. Fukuda, T. Maekawa, T. Hasumura, N. Rantonen, K. Ishii, Y. Nakajima, T. Hanajiri, Y. Yoshida, R. Whitby, S. Mikhalovsky, Dissociation of carbon dioxide and creation of carbon particles and films at room temperature, New J. Phys. 9 (2007) 321.

[23] T. Fukuda, K. Ishii, S. Kurosu, R. Whitby, T. Maekawa, Formation of clusters composed of C_{60} molecules via self-assembly in critical fluids, Nanotechnology 18 (2007) 145611.

[24] T. Hasumura, T. Fukuda, R.L.D. Whitby, O. Aschenbrenner, T. Maekawa, Low temperature synthesis of iron containing carbon nanoparticles in critical carbon dioxide, J. Nanopart. Res. 13 (2010) 53–58.

[25] T. Fukuda, Y. Hayasaki, T. Hasumura, Y. Katsube, R.L.D. Whitby, T. Maekawa, Low temperature synthesis of carbon fibres and metal-filling carbon nanoparticles with laser irradiation into near-critical benzene, RSC Adv. 5 (2015) 12671–12677.

[26] K.A. Kobe, R.E. Lynn, The critical properties of elements and compounds, Chem. Rev. 52 (1953) 117–236.

[27] M.T. Vieyra-Eusebio, A. Rojas, Vapor pressures and sublimation enthalpies of nickelocene and cobaltocene measured by thermogravimetry, J. Chem. Eng. Data 56 (2011) 5008–5018.

[28] P. Pouponneau, V. Segura, O. Savadogo, J.-C. Leroux, S. Martel, Annealing of magnetic nanoparticles for their encapsulation into microcarriers guided by vascular magnetic resonance navigation, J. Nanopart. Res. 14 (2012) 1–13.

[29] D. Ugarte, Onion-like graphitic particles, Carbon 33 (1995) 989–993.

[30] N. Aguiló-Aguayo, Z. Liu, E. Bertran, J. Yang, Thermal-induced structural evolution of carbon-encapsulated iron nanoparticles generated by two different methods, J. Phys. Chem. C 117 (2013) 19167–19174.

 http://dx.doi.org/10.1016/j.heliyon.2016.e00171

[31] R. Sergiienko, E. Shibata, A. Zentaro, D. Shindo, T. Nakamura, G. Qin, Formation and characterization of graphite-encapsulated cobalt nanoparticles synthesized by electric discharge in an ultrasonic cavitation field of liquid ethanol, Acta Mater. 55 (2007) 3671–3680.

[32] J. Jiao, S. Seraphin, Carbon encapsulated nanoparticles of N, Co, Cu, and Ti, J. Appl. Phys. 83 (1998) 2442.

[33] T. Fukuda, N. Watabe, R. Whitby, T. Maekawa, Creation of carbon onions and coils at low temperature in near-critical benzene irradiated with an ultraviolet laser, Nanotechnology 18 (2007) 415604.

[34] S.H. Huh, A. Nakajima, Laser synthesis and magnetism of amorphous iron and cobalt carbide nanoparticles with carbon onion, J. Appl. Phys. 99 (2006) 064302.

[35] Y. Hayasaki, T. Fukuda, T. Hasumura, T. Maekawa, Creation of metal-containing carbon onions via self-assembly in metallocene/benzene solution irradiated with an ultraviolet laser, Adv. Nat. Sci.: Nanosci. Nanotechnol. 3 (2012) 035010.

[36] T. Ogawa, M. Kise, T. Yasuda, H. Kawazumi, S. Yamada, Trace determination of benzene and aromatic molecules in hexane by laser two-photon ionization, Anal. Chem. 64 (1992) 1217–1220.

[37] D. Byun, J.I. Zink, Wavelength-dependent photofragmentation and photoionization of gaseous (η^4-cycloocta-1,5-diene)(η^5-cyclopentadienyl)cobalt, lnorg. Chem. 42 (2003) 4308–4315.

[38] S.J. Blanksby, G.B. Ellison, Bond dissociation energies of organic molecules, Acc. Chem. Res. 36 (2003) 255–263.

[39] U. Ray, H.Q. Hou, Z. Zhang, W. Schwarz, M. Vernon, A crossed laser-molecular beam study of the one and two photon dissociation dynamics of ferrocene at 193 and 248 nm, J. Chem. Phys. 90 (1989) 4248.

[40] C. Famiglietti, E. Baerends, An LCAO HFS investigation of the electronic structure of cobaltocene, Chem. Phys. 62 (1981) 407–421.

[41] J.B. Park, S.H. Jeong, M.S. Jeong, J.Y. Kim, B.K. Cho, Synthesis of carbon-encapsulated magnetic nanoparticles by pulsed laser irradiation of solution, Carbon 46 (2008) 1369–1377.

[42] V.M. Khot, A.B. Salunkhe, N.D. Thorat, R.S. Ningthoujam, S.H. Pawar, Induction heating studies of dextran coated $MgFe_2O_4$ nanoparticles for magnetic hyperthermia, Dalton Trans. 42 (2013) 1249–1258.

 http://dx.doi.org/10.1016/j.heliyon.2016.e00171